

1 **Evaluation of atmospheric model parameterization
2 schemes with river network routing and streamflow
3 observations: A case study of the Yarlung Zangbo
4 River on the Tibetan Plateau**

5 **Heng Yang¹, Shuanglong Chen², Qingyun Bian³, and Hui Zheng⁴**

6 ¹Science and Technology Research Institute, China Three Gorges Corporation, Beijing 100038, China

7 ²Baihetan Hydropower Plant, China Three Gorges Corporation, Sichuan 615421, China

8 ³IEIT Systems Co., Ltd., Beijing 100095, China

9 ⁴Institute of Atmospheric Physics, Chinese Academy of Sciences, Beijing 100029, China

10 **Key Points:**

- 11 • A river network routing-based method is developed to evaluate atmospheric mod-
12 els using streamflow observations
- 13 • High skill in streamflow correlation coefficient corresponds to superiority in mod-
14 eling the spatial distribution of precipitation
- 15 • Shortwave radiation parameterization has a minimal impact on precipitation es-
16 timation but a notable impact on runoff and streamflow

Abstract

Evaluating kilometer-scale atmospheric models in data-sparse regions with complex topography, such as the Tibetan Plateau, presents inherent challenges due to the scarcity of in-situ observations and uncertainties in remote-sensing data. Hydrological evaluation, which utilize hydrological models to connect atmospheric model-simulated precipitation with streamflow observations, are hindered by model structural and parameter uncertainties, particularly significant in high-altitude mountainous basins. This study introduces a river network routing-based method that calculates streamflow directly from atmospheric model-simulated runoff, making fewer assumptions and thus being more adaptable to high-altitude mountainous basins. We applied this method to assess 3-kilometer Weather Research and Forecasting model simulations over the Yarlung Zangbo River on the Tibetan Plateau, each configured with distinct parameterizations for microphysics, planetary boundary layer, and shortwave radiation. The streamflow evaluation was compared with an evaluation of precipitation against satellite data. Results indicate that the streamflow evaluation complements the precipitation evaluation effectively. The WRF simulation that excelled in reproducing precipitation amounts and temporal variations also demonstrated the best performance in estimating streamflow's mean and variability. Furthermore, the river routing-based evaluation of streamflow offers additional insights beyond the precipitation evaluation. While the shortwave radiation parameterization had negligible impacts on precipitation amount, its influence on streamflow was significant. The experiment utilizing the Dudhia radiation scheme achieved the best temporal correlation with streamflow observations, corresponding to an accurate representation of spatial precipitation patterns as evaluated against satellite data. The findings underscore the value of the river network routing-based method in evaluating atmospheric models, especially in data-sparse and topographically complex regions.

1 Introduction

In recent years, the resolution of atmospheric models has gradually increased, reaching grid spacings as fine as 5 kilometers or less. These high-resolution, kilometer-scale models have largely overcome the need for deep convection parameterizations, thereby eliminating a significant source of uncertainty that was previously inherent in coarser-resolution models (Prein et al., 2015; Mooney et al., 2017). Moreover, kilometer-scale atmospheric simulations are capable of capturing the intricate effects of fine-scale topog-

49 raphy on atmospheric circulation patterns, particularly in mountainous regions (C. Lin
50 et al., 2018; Zhou et al., 2021; Yuan et al., 2023; Sugimoto et al., 2021; Ma et al., 2023;
51 Li et al., 2022). The explicit representation of deep convection and meticulous attention
52 to topographic detail have substantially enhanced the accuracy of the estimation of hy-
53 drological gradient along terrain slopes (Jiang, Yang, Yang, et al., 2022; Sugimoto et al.,
54 2021; Ma et al., 2023).

55 In mountainous regions characterized by strong hydrological gradients, such as the
56 Tibetan Plateau, kilometer-scale atmospheric models are particularly useful (Prein et
57 al., 2023). Mountainous regions experience pronounced hydrological gradients (Immerzeel
58 et al., 2014) that are undergoing substantial changes due to global climate change (Yao
59 et al., 2019; Cui et al., 2023; T. Wang et al., 2021; Kraaijenbrink et al., 2021). The scarcity
60 of in-situ observations and the inherent uncertainties in remote-sensing products impede
61 the accurate monitoring of these hydrological changes (Miao et al., 2024). Evidence sug-
62 gests that kilometer-scale atmospheric models can achieve an accuracy that surpasses
63 that of in-situ observations (Lundquist et al., 2019) and even satellite-based products
64 (Jiang, Yang, Li, et al., 2022). Moreover, these models are indispensable for projecting
65 future water resources in the context of a changing climate (Prein et al., 2023).

66 In mountainous regions, accurately evaluating kilometer-scale atmospheric mod-
67 els presents a formidable challenge. Meteorological observations are frequently confined
68 to select locations within river valleys, leaving vast areas unmonitored. Remote locales,
69 such as mountain peaks and barren lands, are known to contribute significantly to wa-
70 ter sources but are often overlooked in observational data (Miao et al., 2024). The com-
71 plex topography and frozen ground in these areas can significantly distort remote-sensing
72 products, including satellite-based precipitation estimates (Behrangi et al., 2014). Con-
73 sequently, the scarcity of in-situ meteorological observations and the associated uncer-
74 tainties in remote-sensing data render the assessment of kilometer-scale atmospheric mod-
75 els less conclusive.

76 The concept of "doing hydrology backward" (Kirchner, 2009) has offered an en-
77 lightening method for evaluating atmospheric models in mountainous regions. This method
78 involves using the precipitation simulated by an atmospheric model to drive a hydrolog-
79 ical model, and then comparing the resulting streamflow with observed streamflow (Krier
80 et al., 2012; Henn et al., 2015, 2016; Pang et al., 2020). However, employing a hydro-

logical model necessitates a substantial set of assumptions regarding model structure and parameters (Kirchner, 2009; Henn et al., 2016). These assumptions can be tested in data-rich regions (Clark et al., 2011; Zheng et al., 2020) but may falter in data-sparse regions, such as the Tibetan Plateau. To encompass the model's structural and parameter uncertainties, a diverse ensemble of model runs is essential to capture the spectrum of possible outcomes (Henn et al., 2015; Vrugt et al., 2008). Yet, there exists the possibility that such uncertainties could be so pronounced that deriving precipitation from streamflow becomes an ill-posed problem (Renard et al., 2010). This concern is particularly pertinent to high-altitude mountainous basins, such as the Yarlung Zangbo River basin, where considerable model structural and parameter uncertainty has been found in our previous study (Lei et al., 2024).

Despite the intricate nature of runoff-generation processes in mountainous regions (van Tiel et al., 2024), the dynamics of water flow are often less complex than those observed over flat terrains (Getirana & Paiva, 2013; Moussa & Bocquillon, 1996). Characterized by steep slopes, mountain rivers enable water flow to be primarily represented using the kinematic wave approximation of the Saint-Venant equations (Moussa & Bocquillon, 1996). This representation indicates that the flow is predominantly influenced by the interplay between friction and channel slope (Getirana & Paiva, 2013; Moussa & Bocquillon, 1996). Given that river channel slopes can be extracted globally from high-resolution digital elevation models (Yamazaki et al., 2017, 2019), the routing of water flow in mountainous basins is heavily reliant on assumptions about channel friction. While the friction assumption makes a relatively minor component within the previously discussed hydrological models, characterizing uncertainties in channel friction is often more straightforward than addressing the structural and parameter uncertainties inherent to hydrological models. The simplicity and robustness of the routing process in mountainous basins enhance its adaptability for evaluating atmospheric models in these regions.

In the light of the aforementioned findings, we propose an alternative approach to evaluating atmospheric models that leverages river network routing. This approach involves directly routing the runoff simulated by atmospheric models through the river network to generate streamflow estimates at gauge locations. The method streamlines the evaluation process by circumventing the complexities of runoff generation processes, which are now integrated within the atmospheric model. The atmospheric models are capable of more effectively constraining the runoff generation processes than hydrological mod-

els, due to their ability to account for surface energy and water balance dynamics as well as land-atmosphere interactions (Wagner et al., 2016; Senatore et al., 2015). We contend that this river network routing-based method is particularly well-suited for data-sparse and topographically complex regions such as the Tibetan Plateau, providing a more targeted and effective means of model evaluation.

In this study, we have implemented our proposed method to evaluate the simulations produced by the Weather Research and Forecasting (WRF) model (Powers et al., 2017), specifically applied to the Yarlung Zangbo River, the most significant river on the Tibetan Plateau. The structure of this paper is as follows: Section 2 delineates the methodologies and datasets utilized within our research. Section 3 details the outcomes and ensuing discussions. Finally, Section 4 synthesizes the findings and concludes the study.

2 Methods and Data

2.1 Experimental Design

Figure 1 illustrates the workflow of this study. We conducted a series of five 3-kilometer WRF experiments from May 1 to October 1, 2013, encompassing the wet season of the year. The experiments were configured with various parameterization schemes for cloud physics, planetary boundary layer, and shortwave radiation. The objective was to identify the optimal parameterization scheme using the streamflow observations from four river gauges along the Yarlung Zangbo River, namely Lazi, Nugesha, Yangcun, and Nuxia, arranged from upstream to downstream.

The WRF experiments were initialized and driven by data from the European Centre for Medium-Range Weather Forecasts Reanalysis version 5 (ERA5) (Hersbach et al., 2020). Following this, the runoff simulated by WRF was spatially re-mapped to account for lateral inflow into the river network. The river flow within this network was then routed using the Muskingum method, a well-established approach for routing mountainous river flows. We tested a range of routing parameter values, calibrating them against streamflow observations to identify the optimal value for each segment of the river network situated between two river gauges. Subsequently, the WRF experiments were intercompared and assessed based on the accuracy of streamflow estimation using these optimal routing parameters.

144 **2.2 Observational Data**

145 We utilized streamflow data provided by the China Three Gorges Corporation, col-
 146 lected at four river gauges along the Yarlung Zangbo River: Lazi, Nugesha, Yangcun,
 147 and Nuxia. Instantaneous streamflow observations were recorded at 00:00 UTC daily from
 148 June 20 to October 1, 2013. These data were instrumental in optimizing the routing pa-
 149 rameter and evaluating the estimated streamflow for the WRF experiments.

150 To intercompare the river network routing-based evaluation of streamflow with the
 151 widely adopted precipitation evaluations based on remote sensing products, we also em-
 152 ployed the Global Precipitation Measurement (GPM) Multi-satellitE Retrievals for GPM
 153 (IMERG) product (Huffman et al., 2019). The IMERG product offers data at a spatial
 154 resolution of 0.1° by 0.1° and a temporal resolution of 30 minutes. We applied bilinear
 155 interpolation to downscale the GPM data to align with the 3-kilometer resolution of the
 156 WRF grid.

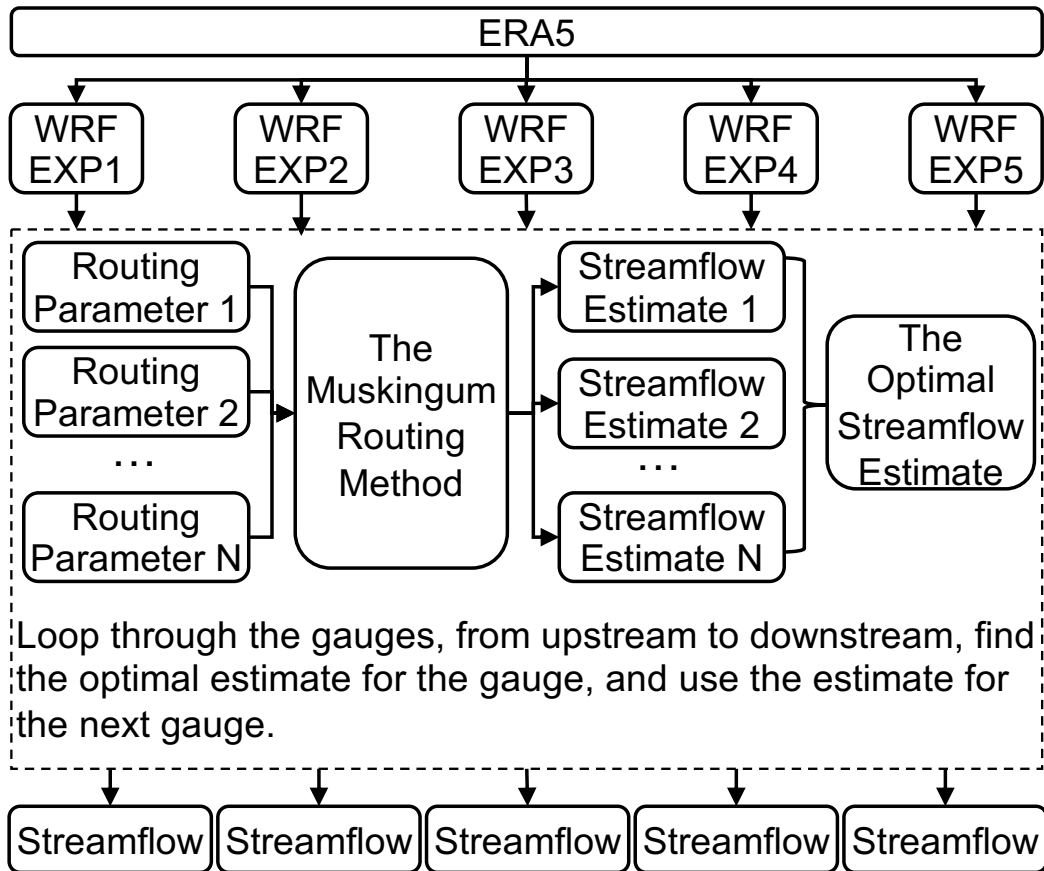


Figure 1. Schematic diagram of the workflow of this study.

157 **2.3 Study Area and River Network**

158 Figure 2 displays the modeling domain of the WRF model, which spans 380 by 660
 159 grid cells, each measuring 3 by 3 kilometers. The domain covers the entire Yarlung Zangbo
 160 River basin and extends to include a buffer zone that surrounds the river basin. This buffer
 161 zone, which is over 200 kilometers wide, is strategically designed to accommodate the
 162 development of small-scale weather systems before they interact with the river basin (Denis
 163 et al., 2002). This design helps to reduce the adverse effects stemming from inaccurate
 164 or low-resolution boundary conditions.

165 The routing was performed on the river network as illustrated in Figure 2. The river
 166 network was delineated from the Multi-Error Removed Improved-Terrain Hydrography
 167 (MERIT-Hydro) dataset (Yamazaki et al., 2017, 2019), which offers flow directions and
 168 accumulative upstream area data at a spatial resolution of 3 by 3 arcseconds. The de-
 169 lineation process unfolds in three sequential steps: Initially, the accumulative upstream
 170 area is employed to identify river centerlines, with a grid cell being classified as such if
 171 its accumulative upstream area surpasses 10 km^2 . Subsequently, these centerlines are seg-
 172 mented into river reaches from upstream to downstream, defining a reach by an increase
 173 in the ccumulative upstream area of at least 20 km^2 along its path. Finally, the flow di-
 174 rection data is utilized to determine the catchment area of each reach, encompassing all
 175 grid cells that contribute flow directly to the reach. The thresholds for defining river cen-
 176 terlines and segmenting river reaches align with those used in previous large-domain river
 177 routing studies (P. Lin et al., 2021, 2019). This delineation process results in a fully con-
 178 nected river network consisting of 5,800 reaches.

179 **2.4 WRF Parameterization Schemes**

180 Table 1 lists the parameterization schemes chosen from WRF version 4.3.1 for the
 181 experiments. EXP1 serves as the baseline experiment, configured similarly to the High
 182 Asian Refined Analysis version 2 (X. Wang et al., 2021) with the exception of the ra-
 183 diation and land surface processes. Instead of the Rapid Radiative Transfer Model (RRTM)
 184 scheme (Mlawer et al., 1997), the RRTM for GCMs (RRTMG) (Iacono et al., 2008) was
 185 employed for shortwave and longwave radiation transfer. RRTMG is comparable to RRTM
 186 in terms of modeling radiative forcing but offers greater computational efficiency (Iacono
 187 et al., 2008). For the land surface processes, the Noah land surface model with multi-

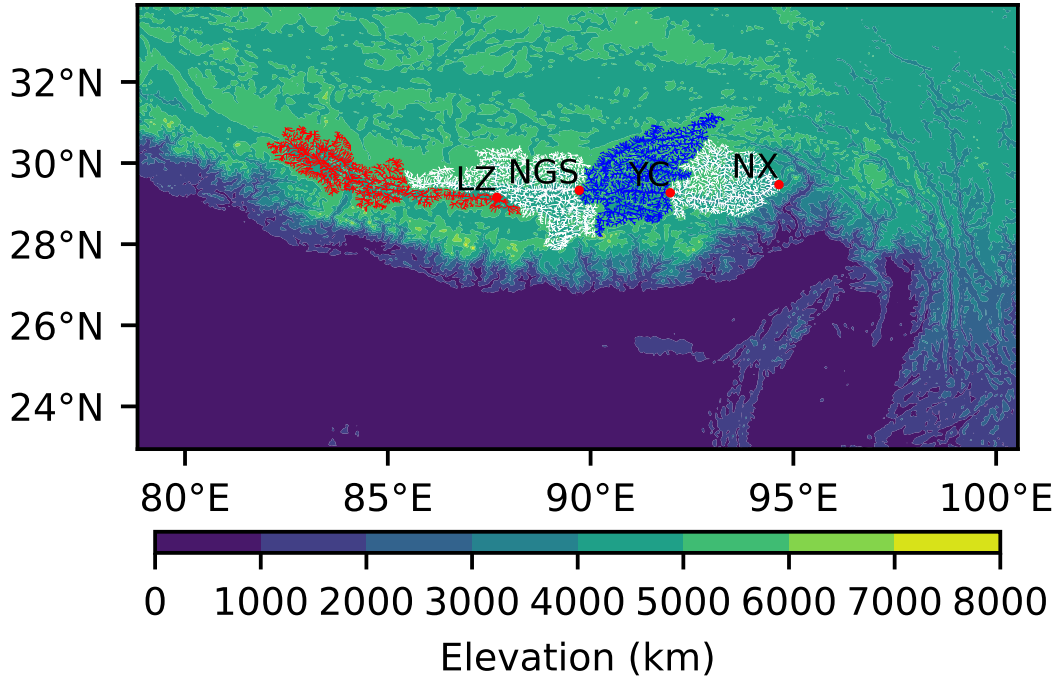


Figure 2. Modeling Domain and Delineated River Network of the Yarlung Zangbo River. The colormap provides a representation of the terrain elevation, showcasing the basin's topographical characteristics. Red dots indicate the locations of the four river gauges along the river's course, labeled as follows: LZ for Lazi, NGS for Nugesha, YC for Yangcun, and NX for Nuxia from upstream to downstream. The differently colored lines correspond to the river reaches that lie between consecutive gauges, offering a visual guide to their spatial distribution across the basin.

parameterization options (Noah-MP) (Niu et al., 2011; Z.-L. Yang et al., 2011) was selected in place of the Noah model used in HARR version 2. Noah-MP has been enhanced over the original Noah model, providing an improved representation of snow and runoff processes (Niu et al., 2011). These enhancements have led to better performance in modeling runoff (Liang et al., 2019; Zheng et al., 2023), leading to the widespread adoption of Noah-MP in hydrological applications (Cosgrove et al., 2024; P. Lin, Hopper, et al., 2018).

Building on EXP1, EXP2 through EXP5 are designed to investigate the impacts of cloud microphysics, planetary boundary layer, and shortwave radiation, one parameterization at a time. These parameterizations have demonstrated their significance in previous studies (Lv et al., 2020; Prein et al., 2023). EXP2 and EXP3 vary from EXP1 in their cloud microphysics schemes. EXP1 employs the Thompson scheme (Thompson

et al., 2008), whereas EXP2 utilizes the Purdue Lin scheme (Chen & Sun, 2002), and EXP3 incorporates the WRF Single-Moment 6-Class Microphysics (WSM6) scheme (Hong & Lim, 2006). EXP4 diverges from EXP1 in its planetary boundary layer scheme. Instead of the Mellor-Yamada-Janjić scheme (Janjić, 1994), EXP4 adopts the Yonsei University scheme (Hong et al., 2006). EXP5 differs from EXP1 in its radiation scheme, opting for the Dudhia scheme (Dudhia, 1989) for shortwave radiation transfer.

Table 1. WRF experiments and the used parameterization schemes.

Experiment	Cloud Microphysics	Planetary Boundary Layer	Shortwave Radiation
EXP1	Thompson	MYJ	RRTMG
EXP2	Purdue Lin	MYJ	RRTMG
EXP3	WSM6	MYJ	RRTMG
EXP4	Thompson	YSU	RRTMG
EXP5	Thompson	YSU	Dudhia

2.5 River Network Routing Method

The WRF-simulated runoff is re-mapped to represent lateral inflow into the rivers, following the remapping method detailed in (P. Lin, Yang, et al., 2018; S. Wang et al., 2019). For each river reach within the network, the WRF grid cells that intersect with the catchment area of the reach are first identified. The runoff volume from these grid cells is then calculated by multiplying the runoff depth by the area of intersection for each cell. These individual values are subsequently summed to ascertain the total lateral flow volume entering the reach. Given the steep topography and extensive watershed area characteristic of the study region, terrain routing is intentionally omitted in this study to focus on the primary river flow dynamics and streamline the computational process.

We employ the Muskingum method to route water flow within the river network. This method is well-suited to characterize the flow's kinematic wave propagation that driven by the topographic gradient (Ponce et al., 1978). The formulation of the Muskingum method (Cunge, 1969; Fenton, 2019), when incorporating lateral inflows, can be

221 expressed as follows:

$$Q_i^t = \frac{k-x}{1-x+k} Q_{i-1}^t + \frac{1-x-k}{1-x+k} Q_i^{t-1} + \frac{x+k}{1-x+k} Q_{i-1}^{t-1} + \frac{2k}{1-x+k} Q_l^t, \quad (1)$$

$$k = \frac{c\Delta t}{2\Delta l}, \quad (2)$$

222 where Q_i^t ($\text{m}^3 \text{s}^{-1}$) is the streamflow of a reach at current time step, Q_{i-1}^t ($\text{m}^3 \text{s}^{-1}$) is the
 223 streamflow at the upstream position of the reach at current time step, Q_i^{t-1} ($\text{m}^3 \text{s}^{-1}$) is
 224 the streamflow of the reach at previous time step, Q_{i-1}^{t-1} ($\text{m}^3 \text{s}^{-1}$) is the streamflow at the
 225 upstream position at the previous time step, Q_l^t ($\text{m}^3 \text{s}^{-1}$) is the lateral inflow entering
 226 the reach at current time step. Δt is the time step (s), and Δl is the reach length (m).
 227 x is the weighting factor (unitless), and c is the wave celerity (m s^{-1}).

228 The application of the Muskingum method to the reaches of a fully connected river
 229 network must be executed in the correct order. When routing the streamflow of a reach,
 230 the discharge at the reach's upstream position must be available. We sorted all the river
 231 reaches with the network according to the stream order as introduced in (X. Yang et al.,
 232 2024). This sorting ensures that upstream reaches are always prioritized over their down-
 233 stream reaches. Subsequently, we apply the Muskingum method to each reach in the es-
 234 tablished sequence. This sequence guarantees that routing on upstream reaches is con-
 235 ducted first, followed by routing on downstream reaches.

236 The Muskingum method includes two adjustable routing parameters: the weight-
 237 ing factor (x ; unitless) and wave celerity (c ; m s^{-1}). The weighting factor x is used to
 238 regulate the proportional contributions of the right-hand-side terms in Equation 1. Stud-
 239 ies have shown that the simulated streamflow is relatively insensitive to variations in the
 240 weighting factor (Koussis, 1978). Values ranging from 0.1 to 0.3 are typically effective
 241 for most streams. Guided by the experiments reported by David et al. (2011), we have
 242 chosen a parameter value of 0.3 for this study.”

243 The wave celerity c represents the speed at which the flow wave propagates down-
 244 stream and is influenced by the physical characteristics of the river channel, including
 245 channel slope, roughness, and width. Given that direct observations of c are unavailable
 246 for the Yarlung Zangbo River basin, we conducted a series of simulations with varying
 247 wave celerity values. We selected the value that best aligns with the streamflow obser-
 248 vations, which is considered representative of the river channel’s physical characteristics.
 249 The optimal wave celerity value c is determined for each streamflow gauge in an upstream-
 250 to-downstream sequence. Once a wave celerity value is chosen for a gauge, it is applied

251 to all downstream gauges. This process is repeated sequentially until wave celerity val-
 252 ues are selected for all streamflow gauges.

253 **2.6 Evaluation Metrics**

254 We utilized the Pearson correlation coefficient to identify the optimal wave celer-
 255 ity value. The Pearson correlation coefficient (r) is defined as follows:

$$r = \frac{\sum_{i=1}^n (x_i - \bar{x})(y_i - \bar{y})}{\sqrt{\sum_{i=1}^n (x_i - \bar{x})^2 \sum_{i=1}^n (y_i - \bar{y})^2}}, \quad (3)$$

256 where x_i and y_i are the simulated and observed streamflow at time step i , respectively.
 257 \bar{x} and \bar{y} are the mean of the simulated and observed streamflow, respectively. The Pear-
 258 son correlation coefficient ranges from -1 to 1 , with a value of 1 indicating a perfect pos-
 259 itive linear relationship between the simulated and observed streamflow. This coefficient
 260 is insensitive to biases in the streamflow estimates, making us to focus on daily scale stream-
 261 flow variations in this study.

262 We used the Kling–Gupta efficiency (KGE) (Gupta et al., 2009) to intercompare
 263 the WRF parameterization schemes. KGE systematically summarizes how a hydrolog-
 264 ical simulation matches observations in correlation, standard deviation, and bias. The
 265 KGE is defined as follows:

$$\text{KGE} = 1 - \sqrt{(r - 1)^2 + (\alpha - 1)^2 + (\beta - 1)^2}, \quad (4)$$

$$\alpha = \frac{\sigma}{\sigma_o}, \quad (5)$$

$$\beta = \frac{\mu_s}{\mu_o}, \quad (6)$$

266 where r is the Pearson correlation coefficient between the simulation and observation,
 267 σ is the standard deviation of the simulation, and μ is the mean. The subscripts s and
 268 o denote the simulated and observed values, respectively. The KGE ranges from $-\infty$ to
 269 1 . A KGE value of 1 indicates a perfect match between the simulated and observed stream-
 270 flow.

271 **3 Results and Discussion**

272 In this section, we first intercompares the WRF-simulated precipitation and runoff.
 273 Subsequently, we assess the streamflow estimates by comparing them against observed
 274 streamflow data.

275 3.1 Intercomparison of the WRF-simulated precipitation and runoff

276 Figure 3 displays the spatial distribution of simulated precipitation from the five
 277 WRF experiments. The patterns from EXP1 through EXP3 exhibit close agreement, with
 278 two primary precipitation centers evident downstream of Yangcun and between Lazi and
 279 Nugesha. Notably, the precipitation intensity between Lazi and Nugesha is slightly higher.
 280 In comparison to the baseline EXP1, the distribution in EXP5 appears more dispersed,
 281 featuring a significant precipitation center downstream of Yangcun, as shown in Figure 3e.
 282 EXP4 closely mirrors the spatial pattern of EXP5, with a spatial correlation coefficient
 283 of 0.93 achieved between them. However, EXP4 (Figure 3d) exhibits the weakest precip-
 284 itation intensity among the experiments. The experiments show greater consensus in the
 285 downstream areas of the Yarlung Zangbo River than in the headwater regions, as indi-
 286 cated in Figure 3f. When juxtaposed with the GPM data, there is a tendency for all five
 287 experiments to overestimate the precipitation rate.

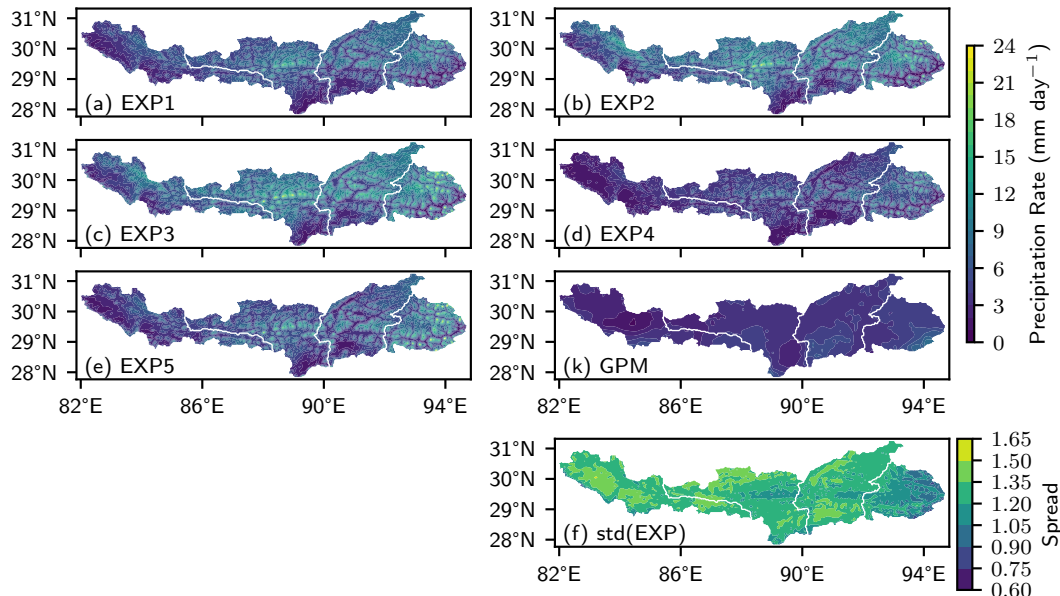


Figure 3. Spatial distribution of the precipitation rate averaged from June 20 to October 1, 2013. (a)–(e) The five WRF experiments described in Table 1. (k) The GPM precipitation. (f) the ensemble spread of the five experiments measured in standard deviation. The white lines denotes the division of the river network between two river gauges.

288 Figure 4 presents the time series of accumulated precipitation, averaged across the
 289 catchments of the four river gauges. Consistent with the spatial distribution depicted

in Figure 3, all five WRF experiments exceed the GPM precipitation rate across all four catchments. The variation among the experiments is considerable. The disparity between EXP4 and EXP1 underscores the significant influence of the planetary boundary layer on precipitation. This finding aligns with the results reported by Prein et al. (2023), suggesting that the impact of planetary boundary layer parameterization can be more pronounced than that of cloud physics, as evidenced by the differences between EXP1 and EXP2, and between EXP1 and EXP3. The difference between EXP5 and EXP1 is negligible across all four catchments, indicating that the parameterization of shortwave radiation has a minimal impact on the simulation of precipitation.

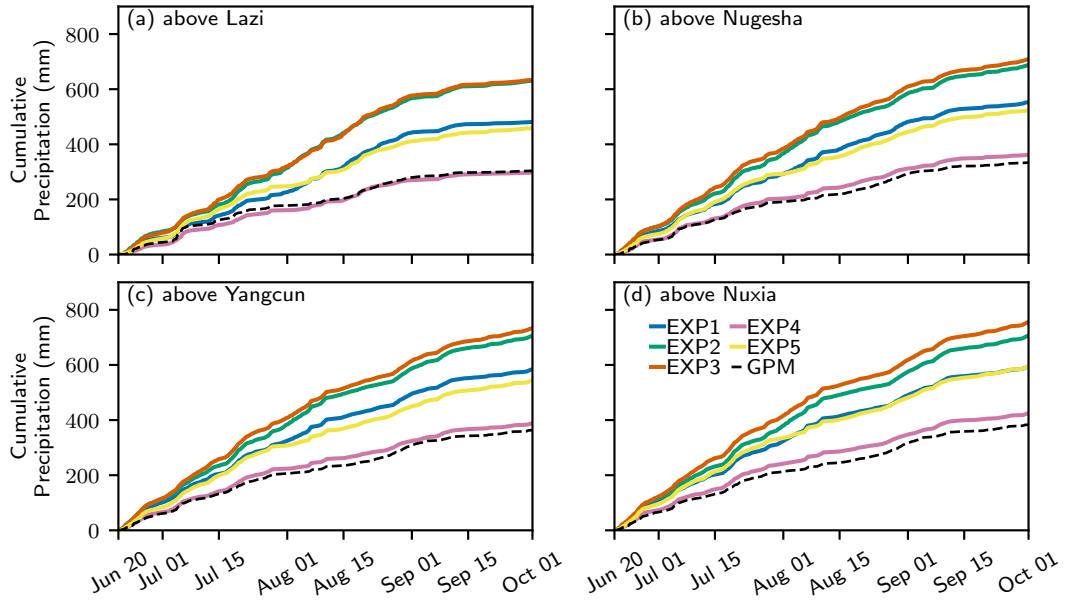


Figure 4. Time series in the accmulated precipitation averaged over the areas above (a) Lazi, (b) Nugesha, (c) Yangcun, and (d) Nuxia.

Table 2 presents the skill of the WRF experiments as measured against GPM data. The cloud physics parameterization significantly influences the timing of precipitation, leading to substantial changes in the correlation coefficient (r) for EXP2 and EXP3 relative to EXP1. A comparison between EXP4 and EXP1 indicates that the planetary boundary layer parameterization has a minimal impact on precipitation timing. However, there are notable differences in the amount of precipitation (β) and its variability (α), suggesting the importance of the planetary boundary layer in moisture transport for precipitation (Y. Wang et al., 2020). Although the shortwave radiation parameterization has

307 a minimal impact on the amount of precipitation (β), it significantly affects the mag-
 308 nitude of precipitation variability (α), particularly in the middle reaches of the Yarlung
 309 Zangbo River between Lazi and Yangcun. The reason for this impact is not yet clear.
 310 However, offline studies in this area (Lei et al., 2024) have found that shortwave radi-
 311 ation significantly affects the land surface energy and water budgets. We hypothesize that
 312 the changes in precipitation may be a consequence of local land-atmosphere interactions
 313 originated from the changes in land surface energy budgets.

314 Figure 5 presents the time series of accumulated runoff, averaged across the catch-
 315 ments of the four river gauges. The accumulated runoff for the specified period corre-
 316 lates well with the precipitation data. The accumulated runoff for the specified period
 317 exhibits a strong correlation with the precipitation data. Among the five experiments,
 318 EXP2 and EXP3 produce the highest runoff estimates, with their performances being
 319 closely aligned. In contrast, EXP4 records the lowest runoff, and its deviation from EXP1
 320 is more significant than the difference observed between EXP1 and EXP2. The dispar-
 321 ity in runoff between EXP5 and EXP1 is considerably larger than the difference in their
 322 respective precipitation estimates, especially in the upper reaches of the Yarlung Zangbo
 323 River, as shown in Figures 5b and 5c. This pronounced difference in runoff is anticipated
 324 to result in variations in the streamflow estimates, which will be further analyzed in the
 325 subsequent sections.

326 **3.2 Evaluation against streamflow observations**

327 Figure 6 demonstrates the changes in the correlation coefficient of streamflow with
 328 celerity across the four river gauges. Table 3 lists the optimal celerity values for each gauge
 329 corresponding to the WRF experiments. The variation of the correlation coefficient with
 330 celerity and the optimal celerity values exhibit consistency across all five experiments.
 331 This consistency supports the notion that celerity is predominantly determined by the
 332 river channel characteristics in mountainous basins. Specifically, the optimal celerity in
 333 the upstream segment of the main channel is generally slower compared to that in the
 334 downstream segment. As shown in Figure 2, the downstream area, located at the edge
 335 of the Tibetan Plateau, is characterized by a broader river channel and a more pronounced
 336 slope, which likely contributes to the observed celerity differences.

Table 2. Kling–Gupta efficiency of the hourly precipitation rate averaged within the catchment of the river gauges. Italic fonts indicate the experiment that best matches GPM.

	Metric	LZ	NGS	YC	NX
EXP1	KGE	0.32	0.25	0.30	0.36
	α	1.06	1.22	1.22	1.22
	β	1.58	1.66	1.60	1.55
	r	0.65	0.72	0.73	0.75
EXP2	KGE	−0.23	−0.22	−0.10	0.00
	α	1.27	1.39	1.37	1.37
	β	2.07	2.06	1.94	1.85
	r	0.46	0.53	0.56	0.60
EXP3	KGE	−0.19	−0.23	−0.12	−0.07
	α	1.22	1.36	1.34	1.34
	β	2.08	2.12	2.01	1.97
	r	0.58	0.65	0.67	0.69
EXP4	KGE	0.61	0.72	0.73	0.75
	α	0.75	0.94	0.94	0.97
	β	0.98	1.09	1.07	1.11
	r	0.70	0.74	0.75	0.77
EXP5	KGE	0.39	0.35	0.42	0.38
	α	0.94	1.11	1.09	1.14
	β	1.51	1.57	1.49	1.55
	r	0.67	0.72	0.71	0.74

Figure 7 displays the time series of streamflow estimates for the five WRF experiments at the four river gauges. Table 4 provides a detailed assessment of the skill of these estimations. Consistent with the observations in precipitation and runoff, there are no

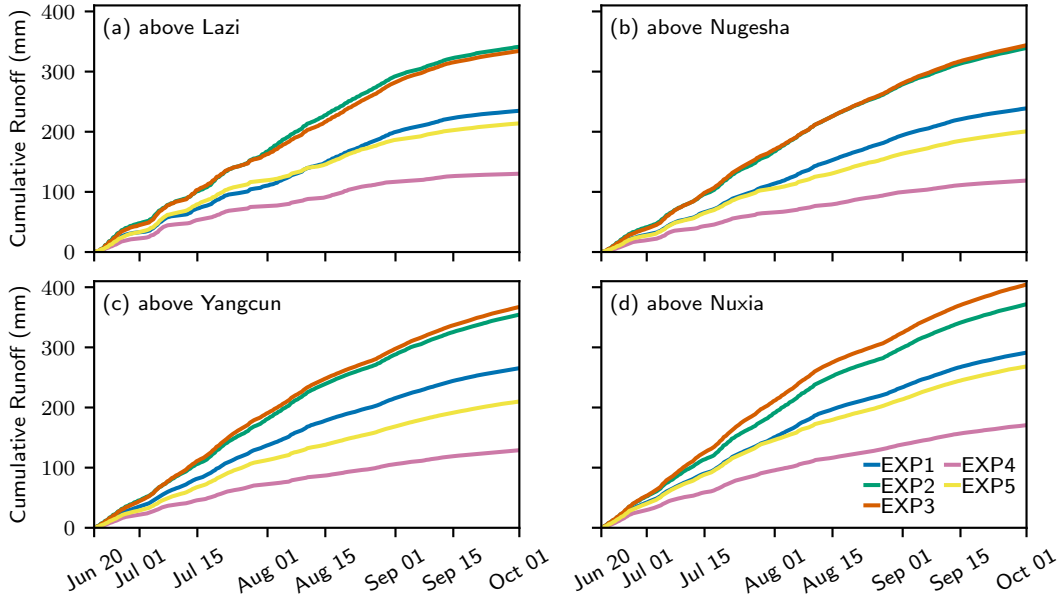


Figure 5. Time series in the accumulated runoff averaged over the areas above (a) Lazi, (b) Nugesha, (c) Yangcun, and (d) Nuxia.

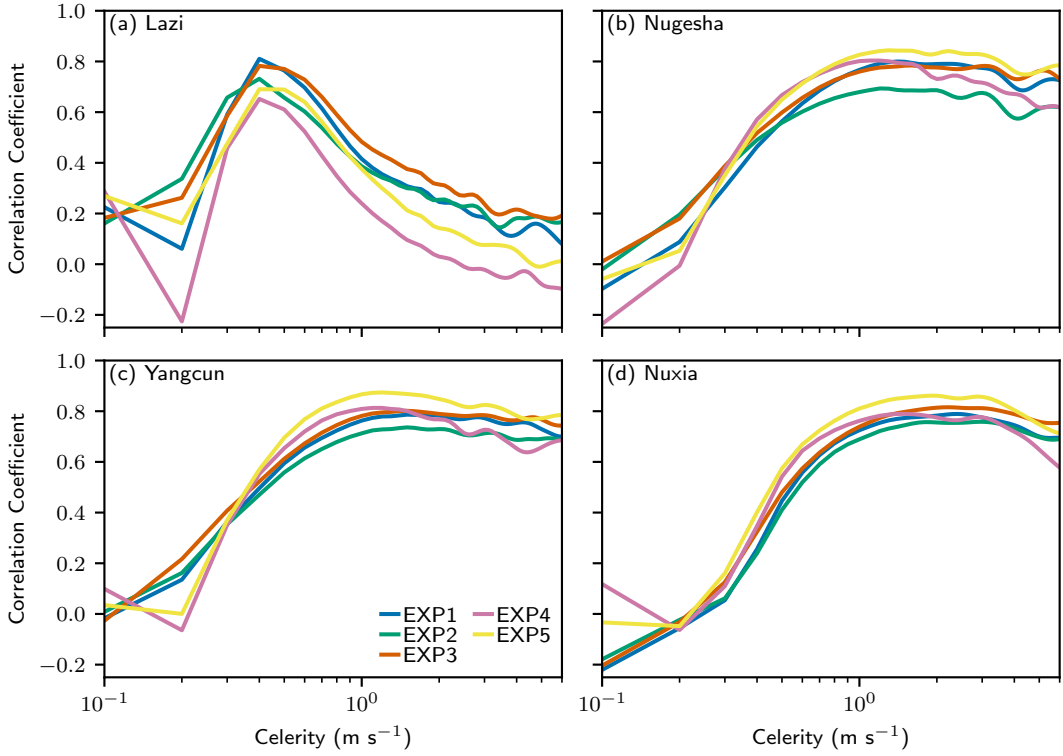


Figure 6. Sensitivity of streamflow modeling skill to wave celerity at the four river gauges.

(a) Lazi, (b) Nugesha, (c) Yangcun, and (d) Nuxia.

Table 3. The optimal flow wave celerity.

	LZ	NGS	YC	NX
EXP1	0.4	1.4	1.5	2.4
EXP2	0.4	1.2	1.5	3.0
EXP3	0.4	1.6	1.5	2.2
EXP4	0.4	1.1	1.2	1.5
EXP5	0.4	1.3	1.2	1.9

table differences in streamflow estimates among the experiments. While EXP4 demonstrated the best performance across all metrics in the evaluation of precipitation against GPM, its advantage in streamflow is primarily observed in terms of bias and in the Kling-Gupta Efficiency (KGE) at the upper to middle reaches. The KGE value for EXP4 increases progressively from upstream to downstream, with a value of -1.78 at the Lazi gauge and improving to 0.69 at the Yangcun gauge. At the most downstream gauge, Nuxia, EXP5 outperforms EXP4, achieving a KGE value of 0.70.

It is noteworthy that EXP5 outperforms EXP1 except at the upstream position of the Yarlung Zangbo River at Lazi, even though their precipitation amounts are quite similar. This superior performance of EXP5 is primarily attributed to the improved correlation coefficient between the simulated and observed streamflow time series. We have examined the relationship between the spatial correlation coefficient of streamflow and the catchment-wide spatial correlation coefficient of precipitation, as depicted in Figure 8. With the exception of the Lazi catchment, a relatively high correspondence in the temporal variations of streamflow is well-aligned with a relatively high correspondence in the spatial distribution of precipitation. This alignment is a consequence of water flow from various locations within the catchment converging at the catchment outlet, which influences the overall streamflow dynamics.

4 Conclusions

We have proposed a river network routing-based method for evaluating atmospheric models using streamflow observations. This method stands out from the hydrological model-

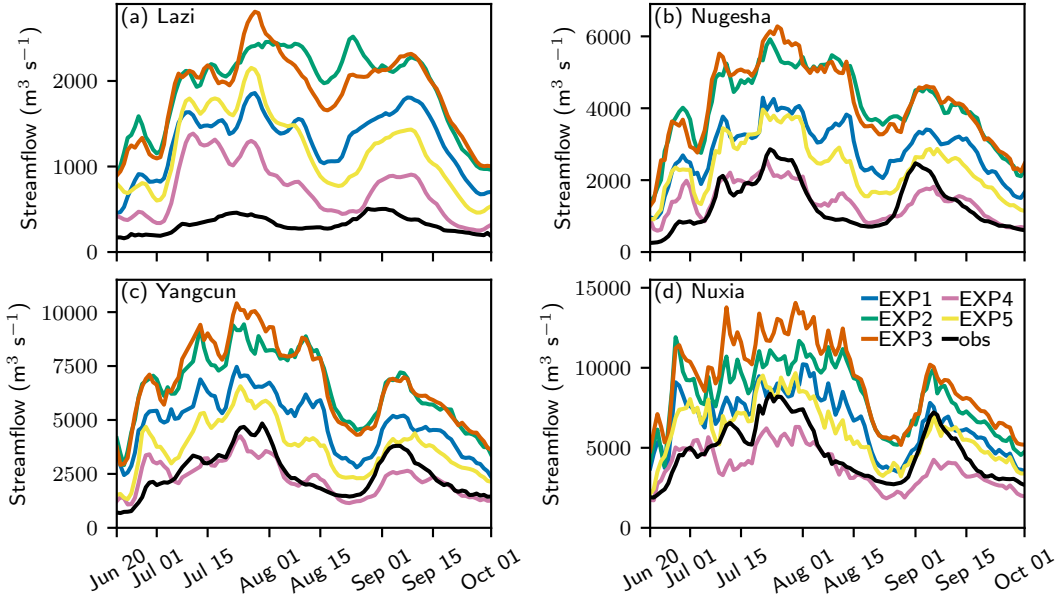


Figure 7. Comparison between streamflow observations and the streaflow estimated from the WRF experiments.

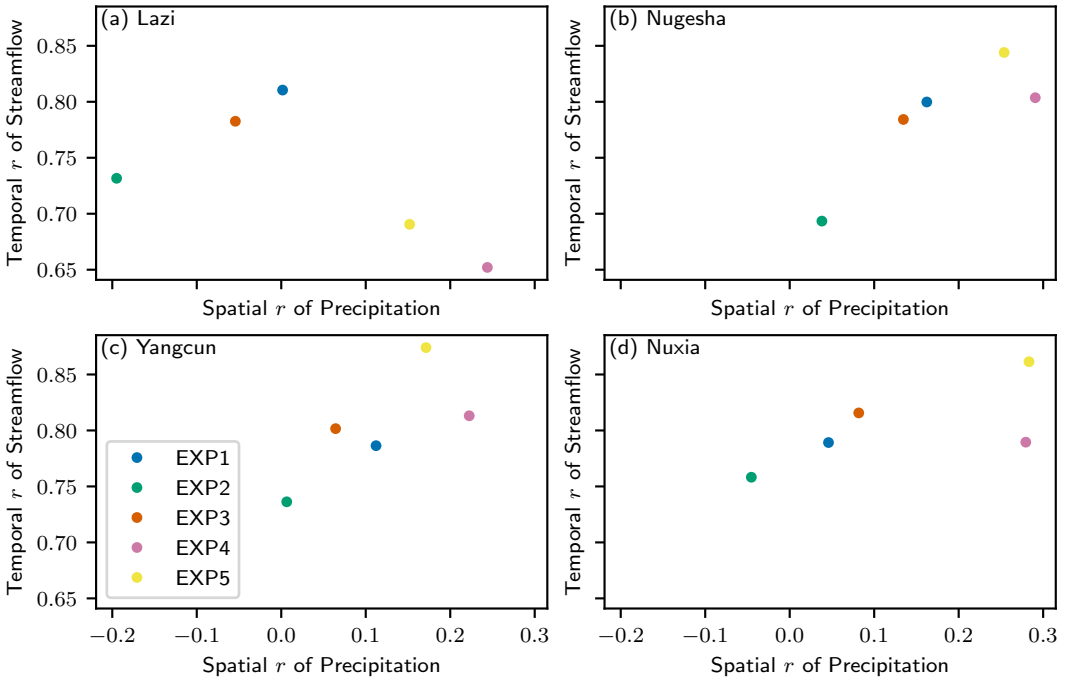


Figure 8. Relationship between the spatial correlation coefficient of precipitation and temporal correlation coefficient of streamflow. (a) The streamflow observed at Lazi and the precipitation averaged in the catchment of Lazi, (b) for Nugesha, (c) for Yangcun, and (d) for Nuxia.

Table 4. Kling–Gupta efficiency of the optimal streamflow estimate.

	Metric	LZ	NGS	YC	NX
EXP1	KGE	-3.12	-0.16	0.01	0.54
	α	3.76	1.14	1.26	1.06
	β	4.05	2.14	1.93	1.40
	r	0.81	0.80	0.79	0.79
EXP2	KGE	-5.34	-1.16	-0.72	0.19
	α	4.88	1.51	1.57	1.23
	β	6.00	3.08	2.60	1.74
	r	0.73	0.69	0.74	0.76
EXP3	KGE	-5.24	-1.21	-0.88	-0.09
	α	4.95	1.65	1.84	1.51
	β	5.82	3.11	2.67	1.95
	r	0.78	0.78	0.80	0.82
EXP4	KGE	-1.78	0.65	0.69	0.60
	α	3.46	0.72	0.77	0.72
	β	2.25	1.07	0.93	0.81
	r	0.65	0.80	0.81	0.79
EXP5	KGE	-3.59	0.19	0.45	0.70
	α	4.71	1.13	1.17	1.04
	β	3.68	1.79	1.51	1.27
	r	0.69	0.84	0.87	0.86

361 based approach by relying on a substantially smaller set of assumptions regarding model
 362 structures and parameters. The streamlined nature of this approach bolsters its robust-
 363 ness and, in comparison to hydrological model-based evaluations, offers a more attrac-
 364 tive alternative. This is especially true in mountainous basins, where the intricacies of

365 runoff-generation processes frequently surpass the modeling capabilities of hydrological
366 models.

367 We applied this method to evaluate five numerical experiments, each featuring dif-
368 ferent configurations of WRF, in the simulated streamflow of the Yarlung Zangbo River,
369 the largest river on the Tibetan Plateau. The streamflow evaluation complements the
370 precipitation evaluation utilizing the GPM precipitation product. Our results indicate
371 a consistency between the proposed method's outcomes and those derived from the pre-
372 cipitation evaluation. Notably, the WRF configuration that integrated the Thompson
373 cloud microphysics scheme, the RRTMG radiation scheme, and the YSU planetary bound-
374 ary layer scheme exhibited optimal performance in simulating precipitation. This con-
375 figuration's enhanced capability to replicate both the total amount and temporal pat-
376 terns of precipitation is crucial for accurately estimating the mean and variability of stream-
377 flow.

378 Our proposed method enriches the evaluation of precipitation. While the shortwave
379 radiation transfer process was found to have a minimal impact on the total amount of
380 precipitation during the initial evaluation, it exerts a significant influence on streamflow
381 simulation, particularly in the middle reaches between Lazi and Yangcun. Notably, the
382 experiment that employed the Dudhia radiation scheme excelled in terms of the corre-
383 lation coefficient and the Kling-Gupta Efficiency (KGE) at the downstream Nuxia gauge.
384 This superior performance in modeling streamflow time series is attributed to the Dud-
385 hia scheme's effectiveness in capturing the spatial distribution of precipitation, under-
386 scoring the importance of accurate radiation transfer modeling in streamflow simulation.
387 These findings reinforce the significance of the precipitation gradient in mountainous hy-
388 drology, as discussed in (Immerzeel et al., 2014), and demonstrate the potential of our
389 proposed method in evaluating atmospheric models in mountainous basins.

390 Open Research Section

391 The GPM precipitation data were retrieved from [https://doi.org/10.5067/GPM/](https://doi.org/10.5067/GPM/IMERG/3B-HH/06)
392 [IMERG/3B-HH/06](https://doi.org/10.5067/GPM/IMERG/3B-HH/06). The ERA5 reanalysis data are obtained from the ECMWF climate
393 data store, accessible via the following DOIs: <https://doi.org/10.24381/cds.bd0915c6>
394 and <https://doi.org/10.24381/cds.adbb2d47>. The WRF model, version 4.3.1, is avail-
395 able at the model's official repository on GitHub: <https://github.com/wrf-model/WRF>.

396 The MERIT-Hydro flow direction and cumulative upstream area data can be accessed
 397 at the following web address: http://hydro.iis.u-tokyo.ac.jp/~yamadai/MERIT_Hydro/.
 398 The delineated river network and WRF-simulated precipitation and runoff can be found
 399 on Science Data Bank (<https://doi.org/10.57760/sciencedb.11618>). The stream-
 400 flow observations for the Yarlung Zangbo River were obtained from China Three Gorges
 401 Corporation; however, they are not shareable due to licensing restrictions. The routing
 402 code used in this study is available at the GitHub repository: <https://github.com/hzheng88/paper-2024-yaluzangbu-wrf-streamflow>.
 403

404 Acknowledgments

405 This study is supported by China Three Gorges Corporation (contract Z532302035)
 406 and the Natural Science Foundation of China (grants 42075165 and 42275178).

407 References

- 408 Behrang, A., Andreadis, K., Fisher, J. B., Turk, F. J., Granger, S., Painter, T.,
 409 & Das, N. (2014). Satellite-based precipitation estimation and its ap-
 410 plication for streamflow prediction over mountainous western U.S. basins.
 411 *Journal of Applied Meteorology and Climatology*, 53(12), 2823–2842. doi:
 412 10.1175/JAMC-D-14-0056.1
- 413 Chen, S.-H., & Sun, W.-Y. (2002). A one-dimensional time dependent cloud model.
 414 *Journal of the Meteorological Society of Japan. Ser. II*, 80(1), 99–118. doi: 10
 415 .2151/jmsj.80.99
- 416 Clark, M. P., Kavetski, D., & Fenicia, F. (2011). Pursuing the method of multi-
 417 ple working hypotheses for hydrological modeling. *Water Resources Research*,
 418 47(9), 1–16. doi: 10.1029/2010WR009827
- 419 Cosgrove, B., Gochis, D., Flowers, T., Dugger, A., Ogden, F., Graziano, T., ...
 420 Zhang, Y. (2024). NOAA's National Water Model: Advancing operational
 421 hydrology through continental-scale modeling. *Journal of the American Water
 422 Resources Association*, 60(2), 247–272. doi: 10.1111/1752-1688.13184
- 423 Cui, T., Li, Y., Yang, L., Nan, Y., Li, K., Tudaji, M., ... Tian, F. (2023).
 424 Non-monotonic changes in Asian Water Towers' streamflow at increas-
 425 ing warming levels. *Nature Communications*, 14(1), 1176. doi: 10.1038/
 426 s41467-023-36804-6

- 427 Cunge, J. A. (1969). On the subject of a flood propagation computation method
 428 (Muskingum method). *Journal of Hydraulic Research*, 7(2), 205–230. doi: 10
 429 .1080/00221686909500264
- 430 David, C. H., Maidment, D. R., Niu, G.-Y., Yang, Z.-L., Habets, F., & Eijkhout, V.
 431 (2011). River network routing on the NHDPlus dataset. *Journal of Hydrometeorology*,
 432 12(5), 913–934. doi: 10.1175/2011JHM1345.1
- 433 Denis, B., Laprise, R., Caya, D., & Côté, J. (2002). Downscaling ability of one-way
 434 nested regional climate models: the Big-Brother Experiment. *Climate Dynamics*,
 435 18(8), 627–646. doi: 10.1007/s00382-001-0201-0
- 436 Dudhia, J. (1989). Numerical study of convection observed during the winter
 437 monsoon experiment using a mesoscale two-dimensional model. *Journal of the Atmospheric Sciences*,
 438 46(20), 3077–3107. doi: 10.1175/1520-0469(1989)
 439 046<3077:NSOCOD>2.0.CO;2
- 440 Fenton, J. D. (2019). Flood routing methods. *Journal of Hydrology*, 570, 251–264.
 441 doi: 10.1016/j.jhydrol.2019.01.006
- 442 Getirana, A. C., & Paiva, R. C. (2013). Mapping large-scale river flow hydraulics
 443 in the Amazon Basin. *Water Resources Research*, 49(5), 2437–2445. doi: 10
 444 .1002/wrcr.20212
- 445 Gupta, H. V., Kling, H., Yilmaz, K. K., & Martinez, G. F. (2009). Decomposition
 446 of the mean squared error and NSE performance criteria: Implications for im-
 447 proving hydrological modelling. *Journal of Hydrology*, 377(1-2), 80–91. doi:
 448 10.1016/j.jhydrol.2009.08.003
- 449 Henn, B., Clark, M. P., Kavetski, D., & Lundquist, J. D. (2015). Estimating moun-
 450 tain basin-mean precipitation from streamflow using Bayesian inference. *Water
 451 Resources Research*, 51(10), 8012–8033. doi: 10.1002/2014WR016736
- 452 Henn, B., Clark, M. P., Kavetski, D., McGurk, B., Painter, T. H., & Lundquist,
 453 J. D. (2016). Combining snow, streamflow, and precipitation gauge observa-
 454 tions to infer basin-mean precipitation. *Water Resources Research*, 52(11),
 455 8700–8723. doi: 10.1002/2015WR018564
- 456 Hersbach, H., Bell, B., Berrisford, P., Hirahara, S., Horányi, A., Muñoz-Sabater, J.,
 457 ... Thépaut, J.-N. (2020). The ERA5 global reanalysis. *Quarterly Journal of
 458 the Royal Meteorological Society*, 146(730), 1999–2049. doi: 10.1002/qj.3803
- 459 Hong, S.-Y., & Lim, J.-O. J. (2006). The WRF Single-Moment 6-Class Microphysics

- 460 Scheme (WSM6). *Asia-Pacific Journal of Atmospheric Sciences*, 42(2), 129–
 461 151.
- 462 Hong, S.-Y., Noh, Y., & Dudhia, J. (2006). A new vertical diffusion package with an
 463 explicit treatment of entrainment processes. *Monthly Weather Review*, 134(9),
 464 2318–2341. doi: 10.1175/MWR3199.1
- 465 Huffman, G. J., Stocker, E. F., Bolvin, D. T., Nelkin, E. J., & Tan, J. (2019).
 466 *GPM IMERG final precipitation L3 half hourly 0.1 degree x 0.1 degree V06*
 467 (*GPM_3IMERGHH*). NASA/GSFC/SED/ESD/GCDC/GESDISC. Retrieved
 468 2022-12-05, from <https://doi.org/10.5067/GPM/IMERG/3B-HH/06> doi:
 469 10.5067/GPM/IMERG/3B-HH/06
- 470 Iacono, M. J., Delamere, J. S., Mlawer, E. J., Shephard, M. W., Clough, S. A., &
 471 Collins, W. D. (2008). Radiative forcing by long-lived greenhouse gases: Cal-
 472 culations with the AER radiative transfer models. *Journal of Geophysical*
 473 *Research: Atmospheres*, 113(D13), D13103. doi: 10.1029/2008JD009944
- 474 Immerzeel, W. W., Petersen, L., Ragettli, S., & Pellicciotti, F. (2014). The impor-
 475 tance of observed gradients of air temperature and precipitation for modeling
 476 runoff from a glacierized watershed in the Nepalese Himalayas. *Water Re-*
 477 *sources Research*, 50(3), 2212–2226. doi: 10.1002/2013WR014506
- 478 Janjić, Z. I. (1994). The step-mountain Eta coordinate model: further developments
 479 of the convection, viscous sublayer, and turbulence closure schemes. *Monthly*
 480 *Weather Review*, 122(5), 927–945. doi: 10.1175/1520-0493(1994)122<0927:
 481 TSMECM>2.0.CO;2
- 482 Jiang, Y., Yang, K., Li, X., Zhang, W., Shen, Y., Chen, Y., & Li, X. (2022).
 483 Atmospheric simulation-based precipitation datasets outperform satellite-
 484 based products in closing basin-wide water budget in the eastern Tibetan
 485 Plateau. *International Journal of Climatology*, 42(14), 7252–7268. doi:
 486 10.1002/joc.7642
- 487 Jiang, Y., Yang, K., Yang, H., Lu, H., Chen, Y., Zhou, X., … Wang, Y. (2022).
 488 Characterizing basin-scale precipitation gradients in the Third Pole region
 489 using a high-resolution atmospheric simulation-based dataset. *Hydrology and*
 490 *Earth System Sciences*, 26(17), 4587–4601. doi: 10.5194/hess-26-4587-2022
- 491 Kirchner, J. W. (2009). Catchments as simple dynamical systems: Catchment char-
 492 acterization, rainfall-runoff modeling, and doing hydrology backward. *Water*

- Resources Research, 45(2), W02429. doi: 10.1029/2008WR006912
- Koussis, A. D. (1978). Theoretical estimation of flood routing parameters. *Journal of the Hydraulics Division*, 104(1), 109–115. doi: 10.1061/JYCEAJ.0004909

Kraaijenbrink, P. D. A., Stigter, E. E., Yao, T., & Immerzeel, W. W. (2021). Climate change decisive for Asia's snow meltwater supply. *Nature Climate Change*, 11(7), 591–597. doi: 10.1038/s41558-021-01074-x

Krier, R., Matgen, P., Goergen, K., Pfister, L., Hoffmann, L., Kirchner, J. W., ... Savenije, H. H. G. (2012). Inferring catchment precipitation by doing hydrology backward: A test in 24 small and mesoscale catchments in Luxembourg. *Water Resources Research*, 48(10), W10525. doi: 10.1029/2011WR010657

Lei, X., Lin, P., Zheng, H., Fei, W., Yin, Z., & Ren, H. (2024). Beyond model parameters: on the meteorological forcing and process parameterization uncertainties in runoff simulation for a poorly-gauged high-altitude river basin. *Journal of Hydrology (under review)*.

Li, G., Chen, H., Xu, M., Zhao, C., Zhong, L., Li, R., ... Gao, Y. (2022). Impacts of topographic complexity on modeling moisture transport and precipitation over the Tibetan Plateau in summer. *Advances in Atmospheric Sciences*, 39(7), 1151–1166. doi: 10.1007/s00376-022-1409-7

Liang, J., Yang, Z.-L., & Lin, P. (2019). Systematic hydrological evaluation of the Noah-MP land surface model over China. *Advances in Atmospheric Sciences*, 36(11), 1171–1187. doi: 10.1007/s00376-019-9016-y

Lin, C., Chen, D., Yang, K., & Ou, T. (2018). Impact of model resolution on simulating the water vapor transport through the central Himalayas: implication for models' wet bias over the Tibetan Plateau. *Climate Dynamics*, 51(9), 3195–3207. doi: 10.1007/s00382-018-4074-x

Lin, P., Hopper, L. J., Yang, Z.-L., Lenz, M., & Zeitler, J. W. (2018). Insights into hydrometeorological factors constraining flood prediction skill during the May and October 2015 Texas Hill Country flood events. *Journal of Hydrometeorology*, 19(8), 1339–1361. doi: 10.1175/JHM-D-18-0038.1

Lin, P., Pan, M., Beck, H. E., Yang, Y., Yamazaki, D., Frasson, R., ... Wood, E. F. (2019). Global reconstruction of naturalized river flows at 2.94 million reaches. *Water Resources Research*, 55(8), 6499–6516. doi: 10.1029/2019WR025287

Lin, P., Pan, M., Wood, E. F., Yamazaki, D., & Allen, G. H. (2021). A new vector-

- 526 based global river network dataset accounting for variable drainage density.
527 *Scientific Data*, 8(1), 28. doi: 10.1038/s41597-021-00819-9
- 528 Lin, P., Yang, Z.-L., Gochis, D. J., Yu, W., Maidment, D. R., Somos-Valenzuela,
529 M. A., & David, C. H. (2018). Implementation of a vector-based river network
530 routing scheme in the community WRF-Hydro modeling framework for flood
531 discharge simulation. *Environmental Modelling & Software*, 107, 1–11. doi:
532 10.1016/j.envsoft.2018.05.018
- 533 Lundquist, J., Hughes, M., Gutmann, E., & Kapnick, S. (2019). Our skill in mod-
534eling mountain rain and snow is bypassing the skill of our observational net-
535 works. *Bulletin of the American Meteorological Society*, 100(12), 2473–2490.
536 doi: 10.1175/bams-d-19-0001.1
- 537 Lv, M., Xu, Z., & Yang, Z. (2020). Cloud resolving WRF simulations of precipi-
538 tation and soil moisture over the central Tibetan Plateau: an assessment of
539 various physics options. *Earth and Space Science*, 7(2), e2019EA000865. doi:
540 10.1029/2019EA000865
- 541 Ma, M., Ou, T., Liu, D., Wang, S., Fang, J., & Tang, J. (2023). Summer re-
542 gional climate simulations over Tibetan Plateau: from gray zone to con-
543 vection permitting scale. *Climate Dynamics*, 60(1), 301–322. doi:
544 10.1007/s00382-022-06314-0
- 545 Miao, C., Immerzeel, W. W., Xu, B., Yang, K., Duan, Q., & Li, X. (2024). Un-
546 derstanding the Asian water tower requires a redesigned precipitation obser-
547 vation strategy. *Proceedings of the National Academy of Sciences*, 121(23),
548 e2403557121. doi: 10.1073/pnas.2403557121
- 549 Mlawer, E. J., Taubman, S. J., Brown, P. D., Iacono, M. J., & Clough, S. A. (1997).
550 Radiative transfer for inhomogeneous atmospheres: RRTM, a validated
551 correlated-k model for the longwave. *Journal of Geophysical Research: At-*
552 *mospheres*, 102(D14), 16663–16682. doi: 10.1029/97JD00237
- 553 Mooney, P. A., Broderick, C., Bruyère, C. L., Mulligan, F. J., & Prein, A. F. (2017).
554 Clustering of observed diurnal cycles of precipitation over the United States
555 for evaluation of a WRF multiphysics regional climate ensemble. *Journal of*
556 *Climate*, 30(22), 9267–9286. doi: 10.1175/JCLI-D-16-0851.1
- 557 Moussa, R., & Bocquillon, C. (1996). Criteria for the choice of flood-routing meth-
558 ods in natural channels. *Journal of Hydrology*, 186(1-4), 1–30. doi: 10.1016/

- 559 S0022-1694(96)03045-4
- 560 Niu, G.-Y., Yang, Z.-L., Mitchell, K. E., Chen, F., Ek, M. B., Barlage, M., ... Xia,
561 Y. (2011). The community Noah land surface model with multiparameteriza-
562 tion options (Noah-MP): 1. Model description and evaluation with local-scale
563 measurements. *Journal of Geophysical Research: Atmospheres*, 116(D12),
564 D12109. doi: 10.1029/2010JD015139
- 565 Pang, J., Zhang, H., Xu, Q., Wang, Y., Wang, Y., Zhang, O., & Hao, J. (2020).
566 Hydrological evaluation of open-access precipitation data using SWAT at mul-
567 tiple temporal and spatial scales. *Hydrology and Earth System Sciences*, 24(7),
568 3603–3626. doi: 10.5194/hess-24-3603-2020
- 569 Ponce, V. M., Simons, D. B., & Li, R.-M. (1978). Applicability of kinematic and dif-
570 fusion models. *Journal of the Hydraulics Division*, 104(3), 353–360. doi: 10
571 .1061/JYCEAJ.0004958
- 572 Powers, J. G., Klemp, J. B., Skamarock, W. C., Davis, C. A., Dudhia, J., Gill,
573 D. O., ... Duda, M. G. (2017). The Weather Research and Forecasting model:
574 overview, system efforts, and future directions. *Bulletin of the American Mete-
575 orological Society*, 98(8), 1717–1737. doi: 10.1175/bams-d-15-00308.1
- 576 Prein, A. F., Ban, N., Ou, T., Tang, J., Sakaguchi, K., Collier, E., ... Chen,
577 D. (2023). Towards ensemble-based kilometer-scale climate simulations
578 over the Third Pole region. *Climate Dynamics*, 60(11), 4055–4081. doi:
579 10.1007/s00382-022-06543-3
- 580 Prein, A. F., Langhans, W., Fosser, G., Ferrone, A., Ban, N., Goergen, K., ... Le-
581 ung, R. (2015). A review on regional convection-permitting climate modeling:
582 Demonstrations, prospects, and challenges. *Reviews of Geophysics*, 53(2),
583 323–361. doi: 10.1002/2014RG000475
- 584 Renard, B., Kavetski, D., Kuczera, G., Thyer, M., & Franks, S. W. (2010). Un-
585 derstanding predictive uncertainty in hydrologic modeling: The challenge of
586 identifying input and structural errors. *Water Resources Research*, 46(5),
587 W05521. doi: 10.1029/2009WR008328
- 588 Senatore, A., Mendicino, G., Gochis, D. J., Yu, W., Yates, D. N., & Kunstmann,
589 H. (2015). Fully coupled atmosphere-hydrology simulations for the central
590 Mediterranean: Impact of enhanced hydrological parameterization for short
591 and long time scales. *Journal of Advances in Modeling Earth Systems*, 7(4),

- 592 1693–1715. doi: 10.1002/2015MS000510
- 593 Sugimoto, S., Ueno, K., Fujinami, H., Nasuno, T., Sato, T., & Takahashi, H. G.
594 (2021). Cloud-resolving-model simulations of nocturnal precipitation over
595 the Himalayan slopes and foothills. *Journal of Hydrometeorology*, 22(12),
596 3171–3188. doi: 10.1175/JHM-D-21-0103.1
- 597 Thompson, G., Field, P. R., Rasmussen, R. M., & Hall, W. D. (2008). Explicit fore-
598 casts of winter precipitation using an improved bulk microphysics scheme. part
599 II: implementation of a new snow parameterization. *Monthly Weather Review*,
600 136(12), 5095–5115. doi: 10.1175/2008MWR2387.1
- 601 van Tiel, M., Aubry-Wake, C., Somers, L., Andermann, C., Avanzi, F., Baraer, M.,
602 ... Yapiyev, V. (2024). Cryosphere–groundwater connectivity is a miss-
603 ing link in the mountain water cycle. *Nature Water*, 2(7), 624–637. doi:
604 10.1038/s44221-024-00277-8
- 605 Vrugt, J. A., ter Braak, C. J. F., Clark, M. P., Hyman, J. M., & Robinson, B. A.
606 (2008). Treatment of input uncertainty in hydrologic modeling: Doing hydro-
607 logy backward with Markov chain Monte Carlo simulation. *Water Resources
608 Research*, 44(12), W00B09. doi: 10.1029/2007wr006720
- 609 Wagner, S., Fersch, B., Yuan, F., Yu, Z., & Kunstmann, H. (2016). Fully coupled
610 atmospheric-hydrological modeling at regional and long-term scales: Devel-
611 opment, application, and analysis of WRF-HMS. *Water Resources Research*,
612 52(4), 3187–3211. doi: 10.1002/2015wr018185
- 613 Wang, S., Zheng, H., Lin, P., Zheng, X., & Yang, Z.-L. (2019). Evaluation and un-
614 certainty attribution of the simulated streamflow from NoahMP-RAPID over a
615 high-altitude mountainous basin. *Chinese Science Bulletin (in Chinese)*, 64(4),
616 444–455. doi: 10.1360/N972018-00598
- 617 Wang, T., Zhao, Y., Xu, C., Ciais, P., Liu, D., Yang, H., ... Yao, T. (2021).
618 Atmospheric dynamic constraints on Tibetan Plateau freshwater under
619 Paris climate targets. *Nature Climate Change*, 11(3), 219–225. doi:
620 10.1038/s41558-020-00974-8
- 621 Wang, X., Tolksdorf, V., Otto, M., & Scherer, D. (2021). WRF-based dynamical
622 downscaling of ERA5 reanalysis data for High Mountain Asia: Towards a new
623 version of the High Asia Refined analysis. *International Journal of Climatol-
624 ogy*, 41(1), 743–762. doi: 10.1002/joc.6686

- 625 Wang, Y., Zeng, X., Xu, X., Welty, J., Lenschow, D. H., Zhou, M., & Zhao, Y.
626 (2020). Why are there more summer afternoon low clouds over the Tibetan
627 Plateau compared to Eastern China? *Geophysical Research Letters*, 47(23),
628 e2020GL089665. doi: 10.1029/2020gl089665
- 629 Yamazaki, D., Ikeshima, D., Sosa, J., Bates, P. D., Allen, G. H., & Pavelsky, T. M.
630 (2019). MERIT Hydro: A high-resolution global hydrography map based on
631 latest topography dataset. *Water Resources Research*, 55(6), 5053–5073. doi:
632 10.1029/2019wr024873
- 633 Yamazaki, D., Ikeshima, D., Tawatari, R., Yamaguchi, T., O'Loughlin, F., Neal,
634 J. C., ... Bates, P. D. (2017). A high-accuracy map of global ter-
635 rain elevations. *Geophysical Research Letters*, 44(11), 5844–5853. doi:
636 10.1002/2017GL072874
- 637 Yang, X., Wei, C., Li, Z., Yang, H., & Zheng, H. (2024). A stream-order family and
638 order-based parallel river network routing method. *Water*, 16(14), 1965. doi:
639 10.3390/w16141965
- 640 Yang, Z.-L., Niu, G.-Y., Mitchell, K. E., Chen, F., Ek, M. B., Barlage, M., ...
641 Xia, Y. (2011). The community Noah land surface model with multipa-
642 rameterization options (Noah-MP): 2. Evaluation over global river basins.
643 *Journal of Geophysical Research: Atmospheres*, 116(D12), D12110. doi:
644 10.1029/2010JD015140
- 645 Yao, T., Xue, Y., Chen, D., Chen, F., Thompson, L., Cui, P., ... Li, Q. (2019).
646 Recent Third Pole's rapid warming accompanies cryospheric melt and wa-
647 ter cycle intensification and interactions between monsoon and environ-
648 ment: multidisciplinary approach with observations, modeling, and analy-
649 sis. *Bulletin of the American Meteorological Society*, 100(3), 423–444. doi:
650 10.1175/bams-d-17-0057.1
- 651 Yuan, X., Yang, K., Lu, H., Wang, Y., & Ma, X. (2023). Impacts of moisture trans-
652 port through and over the Yarlung Tsangpo Grand Canyon on precipitation
653 in the eastern Tibetan Plateau. *Atmospheric Research*, 282, 106533. doi:
654 10.1016/j.atmosres.2022.106533
- 655 Zheng, H., Fei, W., Yang, Z.-L., Wei, J., Zhao, L., Li, L., & Wang, S. (2023). An
656 ensemble of 48 physically perturbed model estimates of the 1/8° terrestrial
657 water budget over the conterminous United States, 1980–2015. *Earth System*

- 658 *Science Data*, 15(7), 2755–2780. doi: 10.5194/essd-15-2755-2023
- 659 Zheng, H., Yang, Z.-L., Lin, P., Wu, W.-Y., Li, L., Xu, Z., ... Wang, S. (2020).
- 660 Falsification-oriented signature-based evaluation for guiding the develop-
- 661 ment of land surface models and the enhancement of observations. *Jour-*
- 662 *nal of Advances in Modeling Earth Systems*, 12(12), e2020MS002132. doi:
- 663 10.1029/2020MS002132
- 664 Zhou, X., Yang, K., Ouyang, L., Wang, Y., Jiang, Y., Li, X., ... Prein, A. (2021).
- 665 Added value of kilometer-scale modeling over the third pole region: a
- 666 CORDEX-CPTP pilot study. *Climate Dynamics*, 57(7), 1673–1687. doi:
- 667 10.1007/s00382-021-05653-8